Journal of Hydroinformatics

Journal of Hydroinformatics Vol 26 No 2, 397 doi: 10.2166/hydro.2024.121

Meteorological characteristics of line-shaped rainbands in northern Japan and its surrounding seas under climate change

Yuta Ohya [a,b,*] and Tomohito J. Yamada [c]

[a] Graduate School of Engineering, Hokkaido University, Sapporo, Hokkaido, 060-8628, Japan
[b] Industrial Technology and Environment Research Department, Research Institute of Energy, Environment, and Geology, Local Independent Administrative Agency Hokkaido Research Organization, Sapporo, Hokkaido 060-0819, Japan
[c] Faculty of Engineering, Hokkaido University, Sapporo, Hokkaido 060-8628, Japan
*Corresponding author. E-mail: ooya-yuuta@hro.or.jp

YO, 0000-0002-4341-0419; TJY, 0000-0002-0031-4283

ABSTRACT

In recent years, line-shaped rainbands (LRBs) have increased in Hokkaido, Japan. LRBs caused several flood disasters historically, thus the weather patterns that cause them need to be investigated. This study aimed to understand statistically the relationship between LRBs and weather patterns during the summer months under climate change conditions. Our study investigates the link between LRBs and weather patterns in Hokkaido during July and August, using historical and climate prediction models. With a 2°/4° global temperature rise, LRB occurrences in this region increase by approximately 1.51/2.07 times. The highest occurrences of LRBs correlate with increased water vapor flux from the south and positive pressure anomalies over the Pacific Ocean. Three main weather patterns contribute significantly to LRBs: (1) a nearby low-pressure system, (2) a strengthening Pacific High frontal pattern, and (3) approaching or landing typhoons in Hokkaido. These patterns double the LRB occurrence probability, a trait observed across past and projected climates (+2K and +4K experiments). These are important insights for future flood risk management.

Key words: climate change, heavy rainfall, line-shaped rainbands, mesoscale, northern Japan, self-organizing maps

HIGHLIGHTS

- Integrative technical approach in hydroinformatics proposed for the first time.
- The novel framework was introduced for the analysis of massive climate data.
- Important new insights into line-shaped rainbands are provided.
- Important insights into the effects of climate change are provided.
- Significant enhancement in understanding summer meteorological fields contributing to heavy rainfall.

GRAPHICAL ABSTRACT

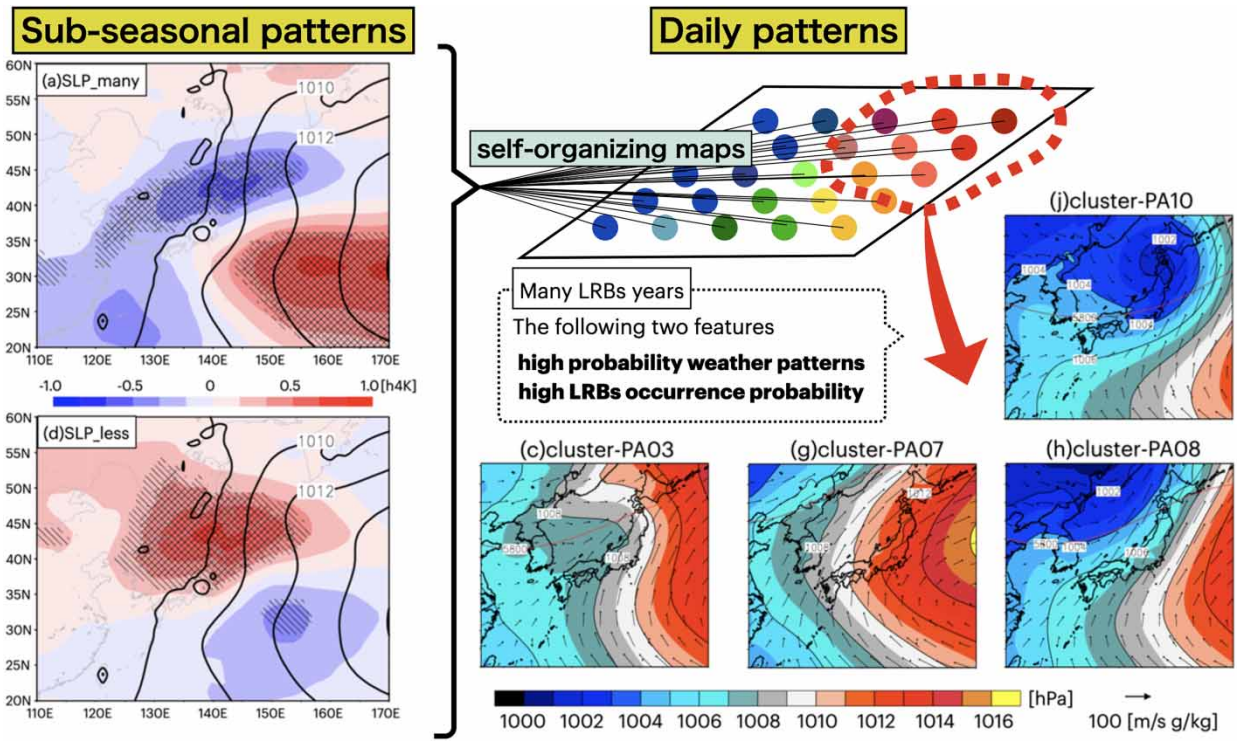

1. INTRODUCTION

In Japan, torrential rainfall frequently occurs during the warm season, from summer to autumn. Flooding and sediment disasters associated with torrential rainfall pose serious issues. Imada *et al.* (2020) show that some historical disasters have increased in risk of torrential rainfall due to climate change. Approximately 50–60% of meso-β-scale rainfall events that are not directly affected by tropical cyclones, including typhoons, are line-shaped (Shimura *et al.* 2000; Tsuguchi & Kato 2014). According to Bluestein & Jain (1985), most line-shaped torrential rains are of the broken-line type or back-building type. However, Ogura (1991) pointed out that most torrential rainfalls occurring in Japan are of the back-building type. Such line-shaped torrential rains are called line-shaped rainbands (hereinafter referred to as 'LRBs'). Back-building LRBs maintain a quasi-steady state by moving the precipitation cell and generating new ones behind it (e.g., Kato 1998, 2006; Yoshizaki *et al.* 2000). The locations where LRBs occur depend on topography and convergence zones in the lower atmosphere (e.g., Takemi 2018; Kato 2020); rainfall areas of LRBs are characterized by rainfall amount, shape, and stagnation, and many of those satisfying threshold values have meso-convective system features (Yamada *et al.* 2012; Unuma & Takemi 2016; Ohya & Yamada 2023).

The number of LRBs has been increasing since 1990 in the Hokkaido region (Yamada *et al.* 2012), the northernmost island of Japan, which was the target of this study. In addition, it has been shown that years with high or low LRBs occurrence are characterized by warm and cold atmospheric circulation conditions with distinct climatological features during July and August (henceforth July–August), which will be discussed in detail later. A related study notes the following weather patterns present on days of LRBs occurrence: stagnant fronts, approaching typhoons, and low-pressure systems passing through the area. The target cases for this study are defined in accordance with Ohya & Yamada (2023). The definition involves smaller rainfall amounts than in other regions of Japan for LRBs. This definition has identified cases with typical back-building events have been identified, such as those that occurred in August 2010 and September 2014 (Yamada *et al.* 2012; Ohya & Yamada 2020). Understanding the specific characteristics of meteorological fields conducive to LRBs occurrence within this region holds critical significance. Moreover, investigating the future shifts in these meteorological attributes due to climate change remains imperative.

This study aims to statistically examine the synoptic meteorological patterns of LRBs during the summer season. First, we verify the characteristics of LRBs previously described by Yamada *et al.* (2012) by utilizing a large ensemble climate dataset.

Note that July–August, when LRBs are concentrated, is the target season. In recent years, the probability of occurrences of some most significant torrential rainfall events with LRBs has increased due to climate change. Osakada & Nakakita (2018) suggest that under future climate conditions, torrential rainfall associated with rainy seasonal fronts may occur in the Hokkaido region, which has not been the case in the past climate simulations. In view of the frequent occurrence of floods and landslides caused not only by typhoons and fronts but also by LRBs, and the further escalation of torrential rainfall associated with climate change, Japan is now considering flood control measures in response to climate change. Aiming to improve flood control safety in river basins, the Ministry of Land, Infrastructure, Transport and Tourism (MLIT) has proposed that the average change in 100-year probable daily rainfall will increase by a factor of 1.1 nationwide and 1.15 regionwide in Hokkaido when the global average temperature increases by 2° in comparison to the pre-industrial era. The above study was conducted using ensemble climate change prediction data from the database for policy decision-making for future climate change (d4PDF; Mizuta *et al.* 2012; Mizuta *et al.* 2017) with coarse horizontal resolutions and the dynamic downscaling of the same data to a horizontal resolution of 5 km. By using high-resolution datasets in this study, we extracted LRBs in the target area and compared them with observations, and future changes in LRBs in the target area were also shown. Then, the characteristics of the seasonal mean synoptic meteorological fields for the years of high and low LRBs occurrence under each climatic condition are described, and the characteristics of the daily synoptic meteorological fields that consist of the period are clarified. Characteristics of the seasonal mean and daily synoptic meteorological fields, which are associated with LRBs, are discussed for both past and future climates, thus making this study a significant novelty.

2. METHODS

2.1. Target area

The area of this study is in Hokkaido, northern Japan, and the surrounding sea area. Figure 1 shows the location and elevation of the target area. We focus on LRBs that occur in the area between 40°–46° north latitude and 138°–146° east longitude,

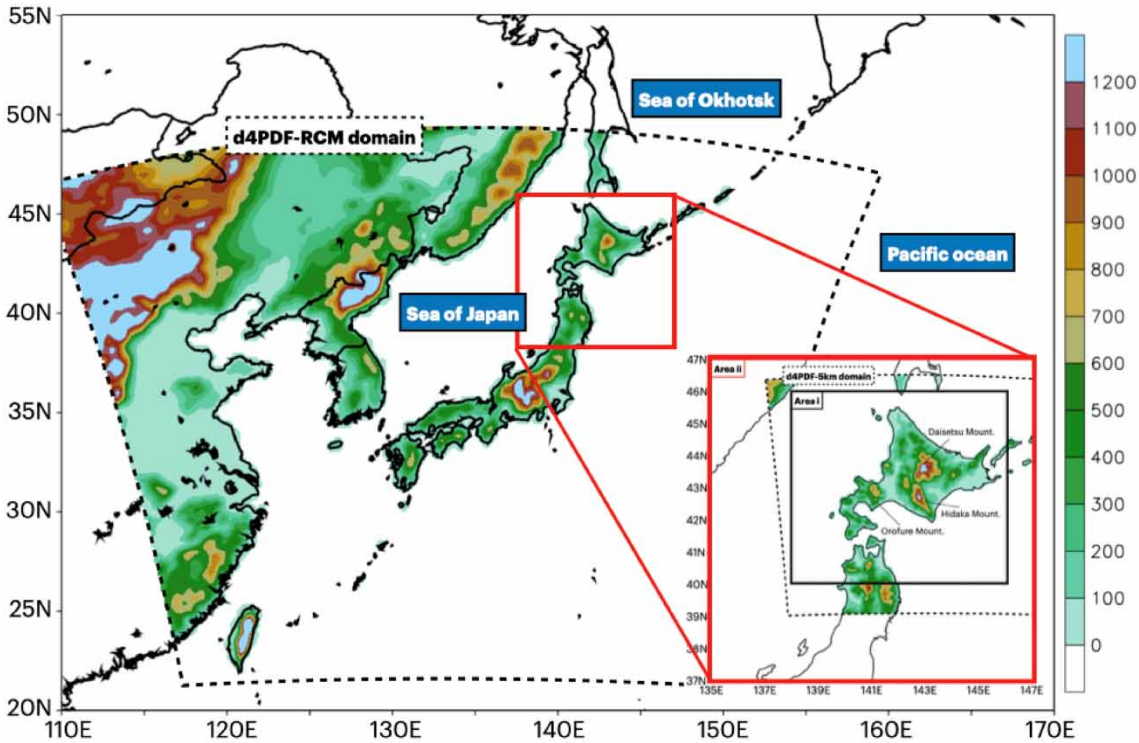

Figure 1 | Overview of the study's target area and elevation (shaded). Map of Japan and surrounding areas. The black dotted line represents the target area for dynamic downscaling from 60 to 20 km spatial resolution using NHRCM. The red box indicates Hokkaido and its surrounding area. The black dotted line within the red box represents the target area for dynamic downscaling from 20 to 5 km spatial resolution using NHRCM. The solid black line indicates the area targeted for LRB extraction.

which is surrounded by a solid black line. The red box in the figure was used for meteorological field classification around northern Japan, and the area surrounded by the black dotted line in the enlarged figure was used to extract LRBs. The Hokkaido Island is surrounded by the Pacific Ocean, the Sea of Japan, and the Sea of Okhotsk. The mountain ranges of Daisetsu, Hidaka, and Olofure with relatively high elevations are characterized by rainfall along the topography brought by typhoons and tropical cyclones moving northward.

2.2. Datasets

In this study, grid-based rainfall data generated from observations and numerical simulations are used. The historical rainfall data are the Radar/Raingauge-Analyzed Precipitation product (Nagata 2011), which is based on radar rain intensity and corrected by ground rain gauges. For past and future climate simulation data, we used 5-km-resolution downscaling datasets from d4PDF (d4PDF-5 km; Yamada *et al.* 2021). d4PDF-5 km is derived from a 20-km-resolution regional experiment (d4PDF-20 km; Mizuta *et al.* 2017). Likewise, d4PDF-20 km is derived from a 60-km-resolution global experiment (d4PDF-60 km; Mizuta *et al.* 2012). Originally, d4PDF-60 km is the simulation data from a global climate model created by adding perturbations to the observational value of sea ice and sea surface temperatures over a 60-year period from 1951 to 2010. The past climate simulations (henceforth the PAST experiments) are based on the observed sea surface temperature (henceforth SST) for 60 years, and they are produced by perturbing of 100 ensemble members, thus producing the equivalent of 3,000 years of data. For the future climate, the observed SST without the interannual trend component is used to add to the global warming effect. The warming effect gives a global mean temperature increase of 2° from the pre-industrial era (the +2 K experiments), corresponding to 2040 in the RCP8.5 scenario. Similarly, a +4 K experiment (i.e., a 4°C increase from pre-industrial times) corresponding to 2090 in the RCP8.5 scenario is also produced. The +2 K/ + 4 K experiments are based on the six representative models (CCSM4, HadGEM2-AO, GFDL-CM3, MRI-CGCM3, MIRM-, MIRM-, and MIRM) selected by cluster analysis of future SST changes in the global atmosphere-ocean coupled models of the Fifth Coupled Model Intercomparison Program (CMIP5). The above 6 SST patterns in the future climate with nine perturbations for +2 K experiments and 15 perturbations for +4 K experiments are applied to the bottom boundary conditions. Since this is also based on 60 years of SST, the data are equivalent to 3,240 and 5,400 years, respectively. The d4PDF-20 km is the result of dynamic downscaling using NHRCM (non-hydrostatic regional climate model; Sasaki *et al.* 2011) of the Meteorological Research Institute in the East Asia region with the above d4PDF-60 km as the lateral boundary condition. Similarly, d4PDF-5 km is the result of dynamically downscaling using NHRCM with d4PD4-20 km as a preliminary boundary condition in Hokkaido and its surrounding waters (Hoshino *et al.* 2020; Yamada *et al.* 2021). For the d4PDF-5 km high-resolution data, 777 years (the PAST experiments), 441 years (the +2 K experiments), and 1,592 years (the +4 K experiments) are available due to the availability of computing resources. The physical processes are the Kain–Fritsch convective parameterization (Kain & Fritsch 1993), and the Mellor–Yamada–Nakanishi–Niino atmospheric boundary layer scheme (closure level: 3; Nakanishi & Niino 2004) was adopted, respectively. The improved MRI/JMA Simple Biosphere (iSiB; Hirai *et al.* 2007) model was used for the land surface processes. The 5-km mesh elevation data are based on the area-averaged elevation. The data have been confirmed to have a high reproducibility of annual maximum rainfall including topographical influences. Although it cannot resolve individual cumulus clouds, the shape and scale of rainfall areas can be inferred from the downscaling results.

2.3. Definition of LRBs

In this study, LRBs were defined as linear and stagnant rainfall areas based on Ohya & Yamada (2023) criteria and were selected from the historical rainfall data and d4PDF-5 km rainfall data if the accumulative rainfall amount in the previous 3 h exceeds 40 mm within a linear stagnant rainfall area, and at least one grid within the rainfall area has rainfall amount of at least 35 mm/h. This rainfall criterion is generally equivalent to related studies in Europe, the U.S., and the tropics (e.g., Nesbitt *et al.* 2006; Fairman *et al.* 2017). However, it includes weaker rainfall events than previous studies in Japan (e.g., Unuma & Takemi 2016; Hirockawa *et al.* 2020). The extraction criteria in previous studies have been found to be insufficient for the Hokkaido region, which is the target of this study. For example, the LRBs that occurred from the Sea of Japan to central Hokkaido in August 2010 (Yamada *et al.* 2012) were not included. Ohya & Yamada (2023) confirmed that this definition can capture the isolated and stagnant linear rainfall systems that have recently occurred in the Hokkaido region, including at least six disaster LRBs. However, the same method sometimes extracts rainfall along the topography of the Hidaka and Daisetsu Mountain ranges as linearly stagnant rainfall. To improve this situation, when 30% of the rainfall area is covered above 700 m elevation, the rainfall is considered topographic rather than LRBs and is removed.

2.4. Classification of meteorological fields

The classification method for the meteorological fields was based on self-organizing maps (hereafter SOM; Kohonen 1982; Kohonen *et al.* 2000), combined with principal component analysis (hereafter PCA) and k-means clustering (e.g., Nguyen-Le *et al.* 2017). SOM has proven to be a suitable match for synoptic meteorology (e.g., Sheridan & Lee 2011). The input information consists of six variables: sea-level pressure (hereafter SLP), geopotential height at 500 hPa, specific humidity at 850 hPa, zonal wind speed, meridional wind speed at 850 hPa, and temperature at 850 hPa. These variables follow Yamada *et al.* (2012) and Nguyen-Le *et al.* (2017), but allow for consideration of the pressure configuration, temperature in the lower layers, and water vapor flux. For the analysis, all grid data for the area in the red box in Figure 1 were used. Therefore, the input dimension of the data is 27,060, which is the number of meteorological variables (6 variables) multiplied by the number of grids (82 east–west grids; 55 north–south grids). The number of input data is based on every 6-hourly output value for each ensemble during the summer (July–August): That is, 4 outputs per day $\times$ 62 days in July–August per year $\times$ 777 years $=$ 192,696-time steps. Since this method is unsupervised learning, all time steps are used as training data. Similarly, there are 109,368-time steps for the +2 K experiments and 394,816-time steps for the +4 K experiments. However, since the meteorological variables or grids are not independent of each other, PCA was first used to reduce the number of dimensions. Furthermore, since the variables used have different dimensions and units, the input information was normalized from 0 to 1 for each grid and each variable. The SOM training information was the top principal component that contributed 85% of the variance of the input data.

The SOM is a nonlinear method for converting the similarity of high-dimensional input data into geometric relationships, and its most important principle is 'learning while preserving the topological relationship between a neuron and its spatial neighbors (neighborhood learning)'. Machine learning was performed by the following process. First, an initialization process randomly assigns initial values to reference vectors to a vector space with a 20 $\times$ 20 geometric arrangement. Next, a competitive process selects the node with the closest distance to the optimal reference vector. Then, a cooperative process calculates the learning weights for the closely located neighboring nodes, weighted by distance and time. Finally, an adaptive process updates the node with the learning amount, and the process is repeated until learning converges. After sufficient learning iterations until convergence, classification into 400 nodes (20 $\times$ 20) was performed, and the composite average of each node was used to classify the meteorological fields into 10 patterns by k-means clustering. This method has been shown to be suitable for analyzing meteorological data because it can adequately represent nonlinear relationships. (e.g., Ohba *et al.* 2016; Nguyen-Le *et al.* 2017). In the case of datasets with a large number of grids and variables (high-dimensional data), such as meteorological data, the computational cost of training and running a machine-learning model can be exorbitantly high. Using only the top few principal components of the PCA as training data, the computational cost can be reduced while efficiently preserving the data variance. Thus, in this paper, this approach has reduced the computational cost to less than 1%.

3. RESULTS AND DISCUSSION

3.1. Frequency of LRBs

Figure 2 shows the spatial distribution of LRBs extracted by the methodology described in section 2.3, normalized as the number of occurrences in each July–August. Figure 2(a) shows the results for the historical 32 years of the historical rainfall data, while Figure 2(b)–(d) shows the results of 777, 441, and 1,592 years from the PAST experiments, the +2 K and +4 K experiments, respectively. The black-colored area in each figure indicates the area where more than 50% of the extracted rainfall areas extend outside of the area of inspection (40–46°N, 138–146°E). This part is excluded from the discussion because it does not allow for equal comparisons. The number of LRBs is higher in the southern part of the region and the western part including the Japan Sea. In future experiments, the number of LRBs will increase in all areas of the target region.

Figure 3 shows the frequency distribution of the number of LRBs in the above areas in July and August. Black indicates the historical rainfall data, blue indicates the PAST experiments, green indicates the +2 K experiments, and red indicates the +4 K experiments. The mean number of LRBs of the +2 K experiments and the +4 K experiments is 1.51/2.08 times higher than that of the PAST experiments. We describe the characteristics of the meteorological fields for the years with many LRBs (hereafter referred to as many LRB years) and the years with few LRBs (hereafter referred to as less LRB years) in each experiment. Many LRB years are defined as the years in which the number of LRBs in July–August is above the 95th percentile of the frequency distribution shown in Figure 3, and less LRB years are defined as the years in which the number of LRBs is below the 5th percentile. Figure 4 shows the average July–August fields of many LRB years

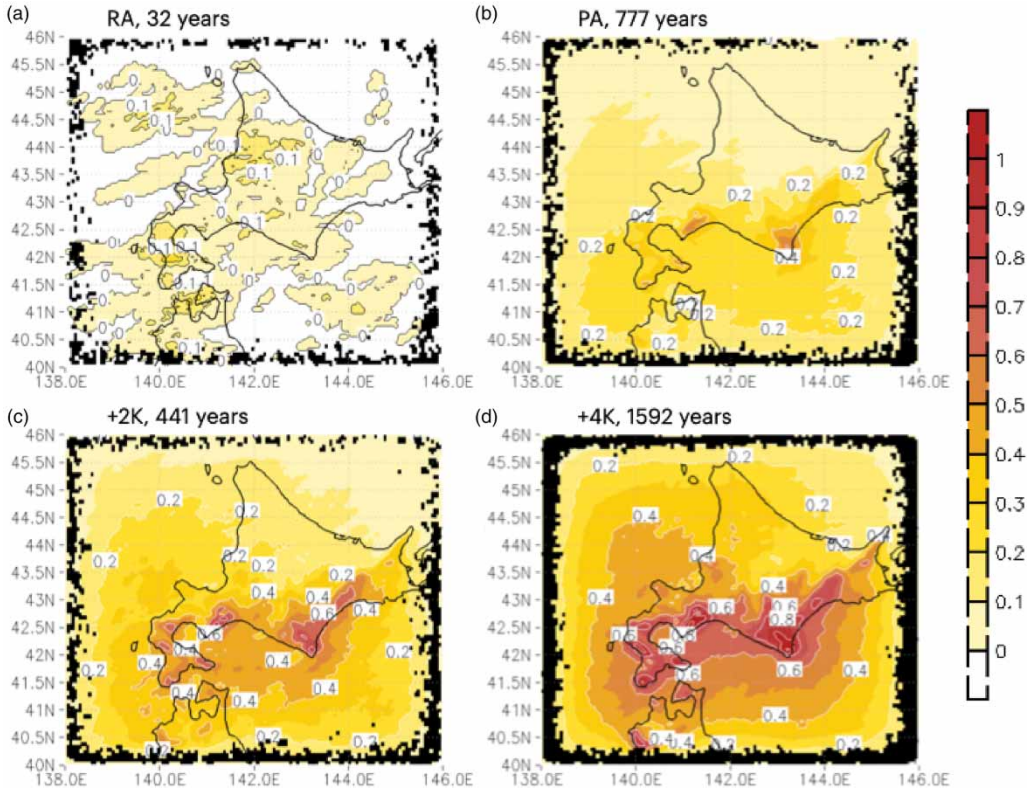

Figure 2 | Number of JA occurrences of extracted LRBs. (a) 32-year average for historical data, (b) 777-year average for the PAST experiments, (c) 441-year average for the +2K experiments, and (d) 1,592-year average for the +4K experiments. (Note that the black areas in each figure represent areas where more than 50% of the rainfall area extends outside the target area.).

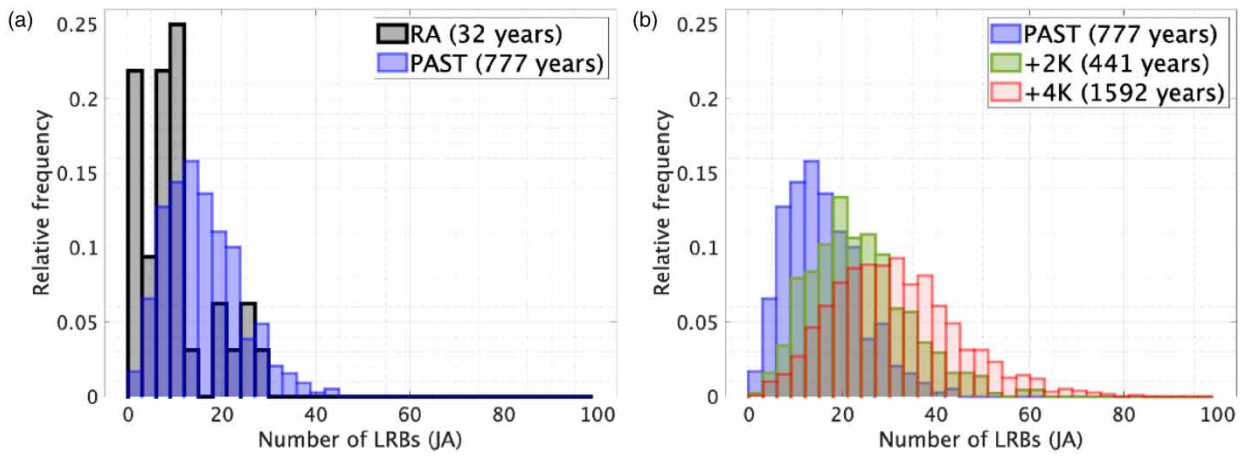

Figure 3 | Frequency distribution of the number of occurrences of LRBs extracted for Hokkaido and its surrounding waters in JA each year. (a) Black represents historical data, and blue represents the PAST experiments, (b) blue represents the PAST experiments, green represents the +2K experiments, and red represents the +4K experiments.

and less LRB years resulting from the 777 years of the PAST experiments. The black lines in the figure indicate the climatological values, and the filled colors indicate the anomaly from the climatological value of the mean of the distribution of many LRB years and less LRB years. The figure with shaded areas where statistical significance levels are satisfied shows that in many LRB years, the low-pressure, tall Pacific High is enhanced around Hokkaido and its western side, and that the

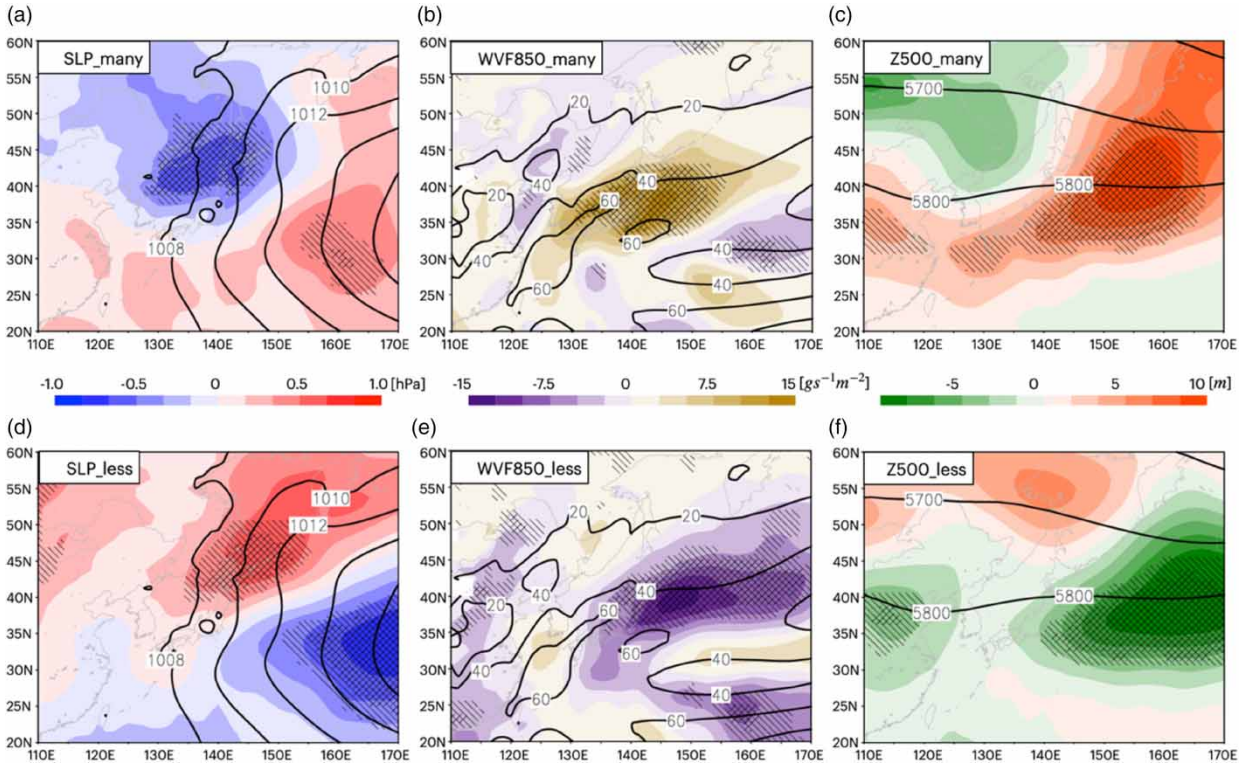

Figure 4 | Climatological values of the PAST experiments (contour) and mean anomalies of many LRB years (the upper row) and less LRB years (the lower row) shown by color shades. (a) Sea-level pressure for many LRB years, (b) water vapor flux at the 850-hPa level for many LRB years, (c) geopotential height at the 500-hPa level for many LRB years, (d) sea-level pressure for less LRB years, and (e) water vapor flux at the 850-hPa surface for less LRB years, (f) geopotential height at the 500-hPa level for less LRB years. (Note that for anomalies, the areas where Welch's *t*-tests showed significant differences of more than 90 and 95% from the climatological values are indicated with single-shaded and double-shaded lines, respectively).

water vapor flux along the extended edge of the high is large. On the other hand, in less LRB years, the development of the Pacific High is suppressed, and the Okhotsk High dominates the northeast of Hokkaido, accompanied by the negative water vapor flux anomalies from the south of the same area.

3.2. Weather pattern classification

Figure 5 shows the classification results for all meteorological data in July–August from the ensemble of 777 years of the PAST experiments. Table 1 shows the characteristics of the weather patterns for each cluster in the classification. The rainy weather pattern clusters are clusters 3, 7, 8, and 10 (PA03, PA07, PA08, and PA10, respectively). PA03 and PA08 are characterized by low-pressure systems approaching Hokkaido, PA07 by a frontal system moving northward or stagnating, and PA10 by an approaching typhoon. On the other hand, the weather pattern clusters with little rainfall are clusters 1, 2, 4, 5, 6, and 9 (PA01, PA02, PA04, PA05, PA06, and PA09, respectively); PA04 is a typical sunny day pattern, and PA09 is a pattern dominated by the Okhotsk Sea High.

3.3. LRBs in each weather pattern

Figure 6 shows the relationship between each weather pattern cluster and LRBs in view of cluster frequency, expected LRBs, and total number of LRBs. The weather patterns that are more likely to occur in many LRB years are PA03, PA07, PA08, and PA10 (Figure 6(a)), which are 1.12, 1.08, 1.32, and 1.22 times more likely to occur in all years, respectively. In contrast, the weather patterns associated with less LRB years are 0.80, 0.86, 0.78, and 0.98 times more likely to occur than all years, respectively. The expected number of LRBs in all years is 0.15, 0.09, 0.20, and 0.23 for the above weather patterns. However, for many LRB years, the expected number of LRBs in the same weather patterns is 0.33, 0.23, 0.32, and 0.42, which is 1.57–2.43 times larger than that of all years. The expected number of LRBs in each weather pattern multiplied by the

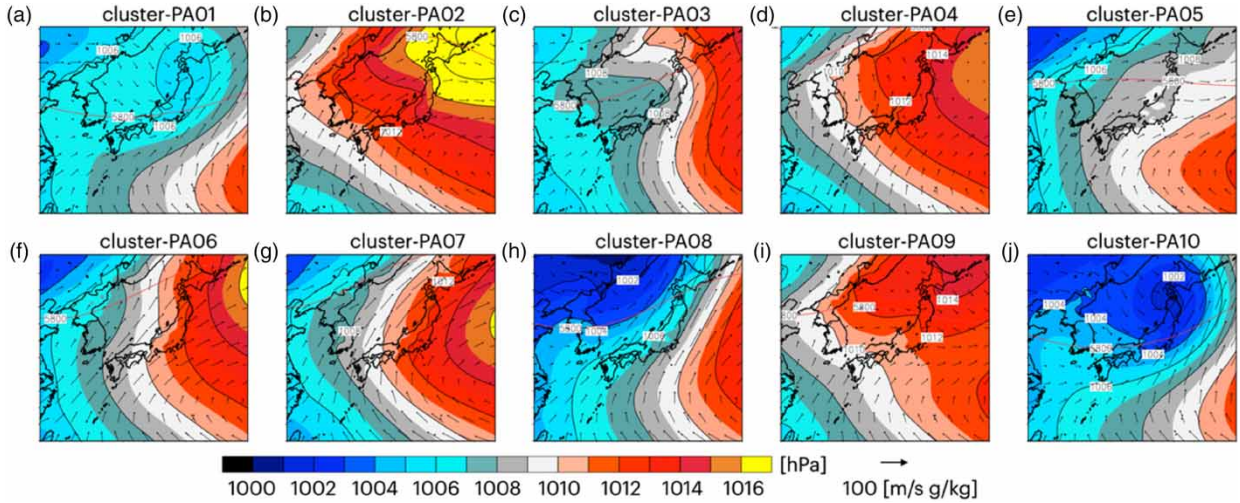

Figure 5 | Composite mean meteorological fields in the PAST experiments cluster. SLP is indicated by shading, and the vector represents water vapor flux (product of specific humidity at 850 hPa and horizontal wind speeds U and V). (a)–(j) correspond to cluster numbers 1–10, respectively.

Table 1 | Characteristics of weather patterns for each cluster in PAST

Cluster	Features of weather patterns
PA01	Low pressure over Hokkaido, but little rainfall tendency.
PA02	High pressure over Hokkaido, little rainfall tendency
PA03	Low pressure over the southwest side of Hokkaido, heavy rainfall tendency in the southern part of Hokkaido
PA04	High pressure over Hokkaido, sunny and hot tendency
PA05	The pressure pattern is moderate, with slightly warmer and little rainfall.
PA06	High pressure over the east side of Hokkaido, and a pressure trough on the west side of Hokkaido, which brings cold air to the west side of the island, causing heavy rainfall in some cases.
PA07	Pacific High pressure strongly extends to the north, and the front tends to move northward, with a tendency of heavy rainfall on the Sea of Japan side.
PA08	The Pacific High is weak, and the low-pressure system moves eastward to Hokkaido, which brings heavy rainfall and high LRBs on the Sea of Japan side.
PA09	The Okhotsk high dominates the area, and the inflow of cold air is strong. Low temperature and little rainfall tendency
PA10	The pressure pattern in which Hokkaido is covered by a low-pressure system, and the number of approaching typhoons is the highest. Heavy rainfall is expected over Hokkaido, especially on the Pacific Ocean side.

occurrence rate of each weather pattern is the total number of LRBs that occur in July–August (Figure 6(c)). Figure 6(c) shows that the total number of LRBs in many LRB years is 2.23 times larger than that in all years. This is due to the combined effects of two factors: (1) the weather patterns favored by LRBs for many LRB years appear to be about 1.08–1.32 times more frequent than that for all years, and (2) the number of LRBs occurrences in the weather pattern for many LRB years is 1.57–2.43 times more frequent than that for all years. In particular, the more significant factor is the increase in the expected number of LRBs in the same weather pattern. In less LRB years, the expected number of LRBs in the same weather patterns is 0.03, 0.01, 0.05, and 0.05, which is 0.09 ~ 0.26 times less than that in all years. The weather patterns most likely to occur in less LRB years are PA09, when the Okhotsk high is strong, and PA02, when the Hokkaido area is covered by a high-pressure system on sunny days. These two weather patterns are 1.65 times and 1.24 times more frequent in less LRB years than in all years, respectively. The results suggest that in many LRB years, the daily weather pattern is characterized by a strong Pacific High and a low-pressure system that often develops around Hokkaido. This pattern is consistent with the characteristic of

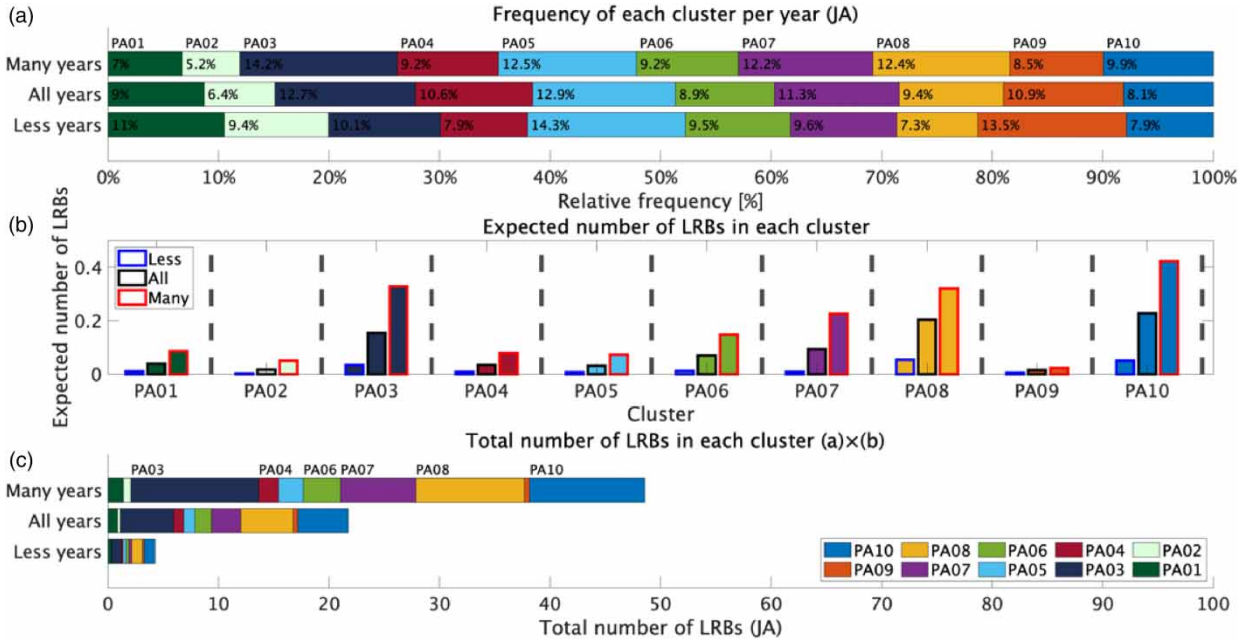

Figure 6 | Occurrence ratio of weather patterns in JA in many LRB years, all years, and less LRB years in the PAST experiments and the number of LRBs during the period. (a) Occurrence ratio of each cluster in the PAST experiments, (b) average number of LRBs for each cluster in the PAST experiments, and (c) total number of LRBs for each cluster in the PAST experiments.

July–August means field. Likewise, in less LRB years, a high-pressure system is often present over Hokkaido and its northern region, which is also consistent with the July–August mean field. While the details are described in the supplementary material, it should be noted that the +2 K experiments and the +4 K experiments also exhibit similar characteristics.

4. CONCLUSIONS

In this study, we examined the relationship between the number of LRBs and meteorological fields in Hokkaido and its surrounding areas during July–August using the historical rainfall data and the past and future climate simulations (the +2 K experiments and the +4 K experiments) from the ensemble climate dataset. We found that the number of LRBs in the target area increased approximately 1.51 times at the +2 K experiments and about 2.07 times at the +4 K experiments compared to the PAST experiments. The potential implication of a significant increase in the number of LRBs is a serious hydrological problem. Specifically, extreme heavy rainfall has been relatively rare in the past, but they become more frequent in recent years. The impact of this is to include torrential events of a previously unexperienced magnitude in the huge number of LRBs. The d4PDF dataset used in this study is based on CMIP5 as the sea surface temperature data. There is currently no apparent difference to CMIP6 in climate repeatability. It is not expected to be a major issue in this study, but it is possible that some differences may be seen in areas prone to precipitation when updated to CMIP6. During many LRB years in each climate scenario, the 2-month mean synoptic field of water vapor flux increases from the south to Hokkaido, which correlates with positive SLP anomalies offshore of the Pacific Ocean. This result is revealed to have statistical significance. These findings are consistent with observations.

Moreover, we analyzed the occurrence characteristics of daily meteorological fields for many LRB years, less LRB years, and all years. Since this method is just a classification of meteorological fields based on the spatial distribution of synoptic scale using key properties, it does not allow us to identify regions or conditions of LRBs occurrences or to mention the dynamical processes in detail. However, as described later, the results are sufficient for a statistical understanding of the frequency of synoptic-scale meteorological patterns. The results revealed that (1) low-pressure patterns, (2) frontal patterns, and (3) typhoon/tropical cyclone patterns, which are more likely to cause LRBs, occurred 1.3 times more frequently in many LRB years compared to all years. The expected number of LRBs occurrences associated with these three weather patterns in many LRB years is more than 1.5 times larger than that in all years. Consequently, the combination of weather patterns

favorable for LRBs occurrences and the high number of LRBs occurrences in those weather patterns contribute to the increased number of LRBs in many LRB years. The +2 K and +4 K experiments also demonstrated a similar relationship between the number of LRBs occurrences and the daily weather patterns. Therefore, understanding the weather patterns likely to cause LRBs, as derived from historical observations, will be valuable for predicting future climate scenarios.

DATA AVAILABILITY STATEMENT

All relevant data are included in the paper or its Supplementary Information.

CONFLICT OF INTEREST

The authors declare there is no conflict.

REFERENCES

Bluestein, H. B. & Jain, M. H. 1985 Formation of mesoscale lines of precipitation: Severe squall lines in Oklahoma during the spring. *Journal of the Atmospheric Sciences* **42** (16), 1711–1732.

Fairman, J. G., Schultz, D. M., Kirshbaum, D. J., Gray, S. L. & Barrett, A. I. 2017 Climatology of size, shape, and intensity of precipitation features over Great Britain and Ireland. *Journal of Hydrometeorology* **18** (6), 1595–1615.

Hirai, M., Sakashita, T., Kitagawa, H., Tsuyuki, T., Hosaka, M. & Oh'Izumi, M. 2007 Development and validation of a new land surface model for JMA's operational global model using the CEOP observation dataset. *Journal of the Meteorological Society of Japan Series II* **85**, 1–24.

Hirockawa, Y., Kato, T., Tsuguti, H. & Seino, N. 2020 Identification and classification of heavy rainfall areas and their characteristic features in Japan. *Journal of the Meteorological Society of Japan Series II* **98** (4), 835–857.

Hoshino, T., Yamada, T. J. & Kawase, H. 2020 Evaluation for characteristics of tropical cyclone induced heavy rainfall over the sub-basins in the central Hokkaido, northern Japan by 5-km large ensemble experiments. *Atmosphere* **11** (5), 435.

Imada, Y., Kawase, H., Watanabe, M., Arai, M., Shiogama, H. & Takayabu, I. 2020 Advanced risk-based event attribution for heavy regional rainfall events. *NPJ Climate and Atmospheric Science* **3** (1), 37.

Kain, J. S. & Fritsch, J. M. 1993 Convective parameterization for mesoscale models: the Kain-Fritsch scheme. In: K.A. Emanuel and D.J. Raymond (Eds.) The representation of cumulus convection in numerical models. Meteorological monographs. Boston: American Meteorological Society, pp. 165–170.

Kato, T. 1998 Numerical simulation of the band-shaped torrential rain observed over southern Kyushu. Japan on 1 August 1993. *Journal of the Meteorological Society of Japan Series II* **76** (1), 97–128.

Kato, T. 2006 Structure of the band-shaped precipitation system inducing the heavy rainfall observed over northern Kyushu. Japan on 29 June 1999. *Journal of the Meteorological Society of Japan Series II* **84** (1), 129–153.

Kato, T. 2020 Quasi-stationary band-shaped precipitation systems, named 'senjo-kousuitai', causing localized heavy rainfall in Japan. *Journal of the Meteorological Society of Japan Series II* **98** (3), 485–509.

Kohonen, T. 1982 Self-organized formation of topologically correct feature maps. *Biological Cybernetics* **43** (1), 59–69.

Kohonen, T., Kaski, S., Lagus, K., Salojarvi, J., Honkela, J., Paatero, V. & Saarela, A. 2000 Self organization of a massive document collection. *IEEE Transactions on Neural Networks* **11** (3), 574–585.

Mizuta, R., Yoshimura, H., Murakami, H., Matsueda, M., Endo, H., Ose, T., Kamiguchi, K., Hosaka, M., Sugi, M., Yukimoto, S., Kusunoki, S. & Kitoh, A. 2012 Climate simulations using MRI-AGCM3.2 with 20-km grid. *Journal of the Meteorological Society of Japan Series II* **90** (0), 233–258.

Mizuta, R., Murata, A., Ishii, M., Shiogama, H., Hibino, K., Mori, N., Arakawa, O., Imada, Y., Yoshida, K., Aoyagi, T., Kawase, H., Mori, M., Okada, Y., Shimura, T., Nagatomo, T., Ikeda, M., Endo, H., Nosaka, M., Arai, M., Takahashi, C., Tanaka, K., Takemi, T., Tachikawa, Y., Temur, K., Kamae, Y., Watanabe, M., Sasaki, H., Kitoh, A., Takayabu, I., Nakakita, E. & Kimoto, M. 2017 Over 5,000 years of ensemble future climate simulations by 60-km global and 20-km regional atmospheric models. *Bulletin of the American Meteorological Society* **98** (7), 1383–1398.

Nagata, K. 2011 Quantitative precipitation estimation and quantitative precipitation forecasting by the Japan Meteorological Agency. *RSMC Tokyo–Typhoon Center Technical Review* **13**, 37–50.

Nakanishi, M. & Niino, H. 2004 An improved Mellor–Yamada level-3 model with condensation physics: Its design and verification. *Boundary-Layer Meteorology* **112**, 1–31.

Nesbitt, S. W., Cifelli, R. & Rutledge, S. A. 2006 Storm morphology and rainfall characteristics of TRMM precipitation features. *Monthly Weather Review* **134** (10), 2702–2721.

Nguyen-Le, D., Yamada, T. J. & Tran-Anh, D. 2017 Classification and forecast of heavy rainfall in northern Kyushu during Baiu season using weather pattern recognition. *Atmospheric Science Letters* **18** (8), 324–329.

Ogura, Y. 1991 Analyses and mechanisms of intense precipitation. *Tenki* **38**, 276–288. (in Japanese).

Ohba, M., Kadokura, S., Nohara, D. & Toyoda, Y. 2016 Rainfall downscaling of weekly ensemble forecasts using self-organising maps. *Tellus A: Dynamic Meteorology and Oceanography* **68** (1), 29293.

Ohya, Y. & Yamada, T. J. 2020 Relationship between vertical vortex structure and precipitation intensity in a line-shaped rain band in Hokkaido in September 2014. *Journal of Japan Society of Civil Engineers, Series B1 (Hydraulic Engineering)* **76** (2), I_193–I_198. (in Japanese).

Ohya, Y. & Yamada, T. J. 2023 Characteristics of line-shaped rainbands regarding duration, shape, and rainfall intensity in northern Japan using the Radar/Raingauge-analyzed precipitation product. In *IOP Conference Series: Earth and Environmental Science*, Vol. 1136, No. 1. IOP Publishing, p. 012025.

Osakada, Y. & Nakakita, E. 2018 Future change of occurrence frequency of Baiu heavy rainfall and its linked atmospheric patterns by multiscale analysis. *Sola* **14**, 79–85.

Sasaki, H., Murata, A., Hanafusa, M., Oh'izumi, M. & Kurihara, K. 2011 Reproducibility of present climate in a non-hydrostatic regional climate model nested within an atmosphere general circulation model. *Sola* **7**, 173–176.

Sheridan, S. C. & Lee, C. C. 2011 The self-organizing map in synoptic climatological research. *Progress in Physical Geography* **35** (1), 109–119.

Shimura, K., Hara, H. & Yamada, T. 2000 Study on generation mechanism and classification of rainfall by the images of Radar Raingauge in the Kanto Plain. *Journal of Japan Society of Civil Engineers, Series B1 (Hydraulic Engineering)* **44**, 97–102. (in Japanese).

Takemi, T. 2018 Importance of terrain representation in simulating a stationary convective system for the July 2017 northern Kyushu heavy rainfall case. *SOLA* **14**, 153–158.

Tsuguchi, H. & Kato, T. 2014 Objective extraction of heavy rainfall events and statistical analysis on their characteristic features. *Tenki* **61** (6), 455–469. (in Japanese).

Unuma, T. & Takemi, T. 2016 Characteristics and environmental conditions of quasi-stationary convective clusters during the warm season in Japan. *Quarterly Journal of the Royal Meteorological Society* **142** (696), 1232–1249.

Yamada, T. J., Sasaki, J. & Matsuoka, N. 2012 Climatology of line-shaped rainbands over northern Japan in boreal summer between 1990 and 2010. *Atmospheric Science Letters* **13** (2), 133–138.

Yamada, T. J., Hoshino, T. & Suzuki, A. 2021 Using a massive high-resolution ensemble climate data set to examine dynamic and thermodynamic aspects of heavy precipitation change. *Atmospheric Science Letters* **22** (12), e1065.

Yoshizaki, M., Kato, T., Tanaka, Y., Takayama, H., Shoji, Y., Seko, H., Arao, K. & Manabe, K. & Members of X-BAIU-98 Observation 2000 Analytical and numerical study of the 26 June 1998 orographic rainband observed in western Kyushu, Japan. *Journal of the Meteorological Society of Japan Series II* **78** (6), 835–856.

First received 15 May 2023; accepted in revised form 10 January 2024. Available online 30 January 2024